Robertson, A.H.F., Emeis, K.-C., Richter, C., and Camerlenghi, A. (Eds.), 1998
Proceedings of the Ocean Drilling Program, Scientific Results, Vol. 160

18. MINERALOGICAL RECORD OF CYCLIC CLIMATE CHANGES IN MEDITERRANEAN MID-PLIOCENE DEPOSITS FROM HOLE 964A (IONIAN BASIN) AND FROM PUNTA PICCOLA (SICILY)[1]

Frédéric Mélières,[2] Alain Foucault,[2] and Marie-Madeleine Blanc-Valleron[2]

ABSTRACT

Mid-Pliocene sediments from Ocean Drilling Program Hole 964A (Ionian Basin) and from Punta Piccola outcrop (Sicily, Italy) consist of light-colored carbonate-rich marls (decimeter to meter thick) alternating with dark-colored, carbonate-poor, organic matter–rich beds (1–25 cm thick). These sediments show cyclic variations in their mineralogical content, especially in the clay mineral relative percentages. Palygorskite and kaolinite are abundant in carbonated intervals, whereas smectite and chlorite dominate in dark ones. As palygorskite is known to originate from Africa, through wind transportation, we interpret these cyclic variations to be a result of the alternation of dry periods, with dominant eolian sedimentary input from the south, and humid periods, with dominant fluvial supply.

INTRODUCTION

Mid-Pliocene sediments recovered from Hole 964A (Fig. 1) of the Ocean Drilling Program (ODP) Leg 160 (Shipboard Scientific Party, 1996) and those of the same age observed in the southern Sicily outcrops of Punta Piccola (Brolsma, 1978; Hilgen, 1987, 1991; Foucault and Mélières, 1995) show similar facies and similar sedimentary cycles, which seem to be controlled by astronomically induced climatic changes (Hilgen, 1991; Lourens et al., 1996). The aim of this study is to analyze these sediments to interpret the cycles in terms of sedimentary and paleoclimate processes.

GEOLOGICAL SETTING

In the Ionian basin, the studied sequence includes sediments from Sections 160-964A-9H-2 through 9H-6, from 97.585 revised meters composite depth (rmcd) to 102.735 rmcd. They are mainly light-colored nannofossil ooze and clayey nannofossil ooze, but dark-colored organic-rich beds (sapropels) alternate with this background lithology. From top to bottom of the studied section, six sapropels were observed, numbered from 50 to 55 (Shipboard Scientific Party, 1996). A gray bed, located between sapropel 51 and sapropel 52 (from 78.53 to 78.62 rmcd), may be interpreted as an oxidized sapropel. As the sediment thickness from sapropel 50 to sapropel 55 is 4.26 m, the mean cycle thickness in the studied section is 0.71 m.

In Sicily, the Punta Piccola section crops out about 8 km west-southwest of Agrigento. The studied section is located in the Monte Narbone Formation and corresponds to cycles 104 to 108 (Hilgen, 1991). It shows mainly light-colored carbonated marls alternating with gray or brown beds whose color is explained by concentration of manganese or organic matter (Brolsma, 1978; Van Os et al., 1994). In this section, mean cycle thickness is 1.75 m, 2.5 times greater than the one calculated for Hole 964A.

Mean sedimentation rates can be calculated using data from Lourens et al. (1996), assuming that the sedimentary cycles were astronomically controlled (2.64 cm·ka^{-1} at Hole 964A; 7.35 cm·ka^{-1} at Punta Piccola). Without higher resolution chronological data, the sedimentation rates cannot be better calculated and are therefore postulated to be constant throughout the cycle duration.

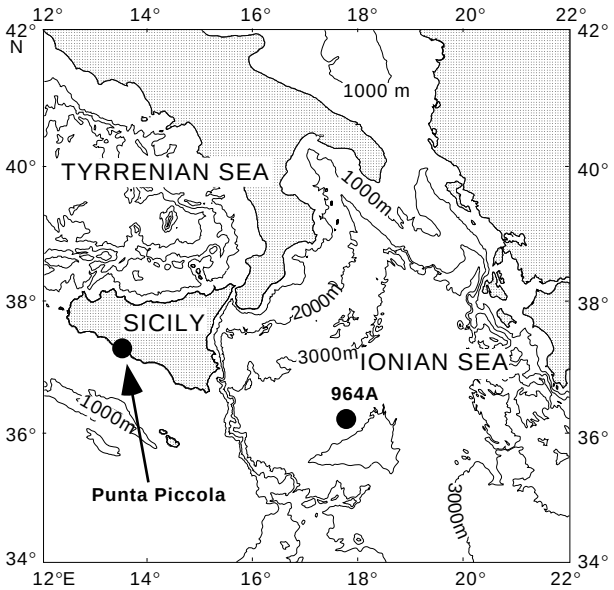

Figure 1. Location of Hole 964A and the Punta Piccola section.

METHODS

At Hole 964A, 102 samples were taken at 5-cm intervals from 97.585 to 102.735 rmcd. This sampling interval is sufficient to characterize the average 71-cm-thick cycles. At Punta Piccola,123 samples were taken every 5 cm. This interval allows us a very good accuracy because of the larger cycles (1.75 m).

Calcareous Nannofossils

Smear slides for light microscope examinations were prepared using standard procedures. A small amount of sediment (5 mm^3) is smeared onto a glass slide using a drop of distilled water and a flat tooth pick. The percentage of *Discoaster tamalis* within a total count of 100 discoasterids is used to correlate Hole 964A with the Punta

[1]Robertson, A.H.F., Emeis, K.-C., Richter, C., and Camerlenghi, A. (Eds.), 1998. *Proc. ODP, Sci. Results*, 160: College Station, TX (Ocean Drilling Program).

[2]Laboratoire de Géologie, Muséum National d'Histoire Naturelle, 43 rue Buffon, 75005 Paris, France. URA 1761 CNRS. foucault@cimrs1.mnhn.fr

Prior Chapter Contents Next Chapter

Piccola section, as it is considered as a good biostratigraphic marker in the Mediterranean (Rio et al., 1990; Channel et al., 1992; Sprovieri et al., 1994).

Mineralogy

Carbonate content was evaluated by manocalcimetry. Quantitative measurements were performed by X-ray diffractometry on a Siemens diffractometer using copper Ni-filtered radiation. The use of a high-speed rotating sample holder (Mélières, 1973) and the systematic duplication of measurements allow a relative accuracy ranging from 2% to 5%. Dolomite, quartz, feldspars, pyrite, and goethite contents were determined on powdered samples, using SiC as internal standard and calibrated curves that take into account the lattice crystallinity. Calcite content is calculated using the relation

$$\% \text{ calcite} = \% \text{ carbonate} - (1.085\% \text{ dolomite}).$$

Clay mineral relative abundances were measured on carbonate-free oriented preparations, using the weighted area of the characteristic diffraction peaks with appropriate quantitative factors. The palygorskite (110) peak area was measured on the glycolated trace after deconvolution of the illite (001)-palygorskite (110) doublet. The chlorite/kaolinite ratio was measured using the chlorite (004)-kaolinite (002) doublet, the abundance of the sum of the two minerals being measured on the unresolved chlorite (002)-kaolinite (001) peak.

STRATIGRAPHICAL CORRELATIONS

The studied sections can be accurately correlated using nannofossil data (Fig. 2). Three bioevents were used, all related to *D. tamalis* (Driever, 1988; Rio et al., 1990; Sprovieri et al., 1994).

1. **Last common occurrence (LCO) of *D. tamalis*.** The LCO of *D. tamalis* was first determined at Sample 160-964A-9H-2, 80 cm (97.08 rmcd), 1.12 m above sapropel 50 (Shipboard Scientific Party, 1996, p. 102, Table 4). Nevertheless, Di Stefano (pers. comm., 1996), locates this LCO between Sample 160-964E-6H-2, 49–51 cm (98.35–98.37 rmcd), 15 cm below the base of the sapropel 50, and Sample 160-964C-9H-6, 65–67 cm (98.09–98.11 rmcd), 11 cm above this base. Our observations (Fig. 2) lead us to locate this LCO in sapropel 50, at 98.185 rmcd. Consequently, the LCO of *D. tamalis* is located in close proximity to the base of sapropel 50.

At Punta Piccola (Brolsma, 1978; Hilgen, 1987, 1991; Driever, 1988), the LCO of *D. tamalis* (biohorizon d9 of Driever, 1988) is located within the base of Driever's cycle number 16 (Driever, 1988), equivalent of Hilgen's cycle 111 (Hilgen, 1991). The position of this biohorizon at Punta Piccola is confirmed by subsequent studies (Sprovieri et al., 1994). We conclude that sapropel 50 of Hole 964A is equivalent to the gray layer located at the base of cycle 111 at Punta Piccola.

2. **Top of *D. tamalis* paracme.** In Hole 964A, the top of the *D. tamalis* paracme was observed (Di Stefano, pers. comm., 1996) in Sample 160-964E-6H-2, 127–129 cm (99.23–99.25 rmcd), 7 cm above the base of sapropel 51. We observed it in this sapropel at 99.285 rmcd (Fig. 2).

In the Punta Piccola section, the top of *D. tamalis* corresponds (Di Stefano, pers. comm., 1996) to Driever's biohorizon d8, just above the sapropel base of the cycle 15 (Driever, 1988), equivalent to Hilgen's cycle 110. We can then conclude that the sapropel 51 in the Hole 964A is equivalent to the base of cycle 110 at Punta Piccola.

3. **Bottom of *D. tamalis* paracme.** In Hole 964A, we observed the bottom of *D. tamalis* paracme at 101.685 rmcd, in sapropel 54 (Fig. 2).

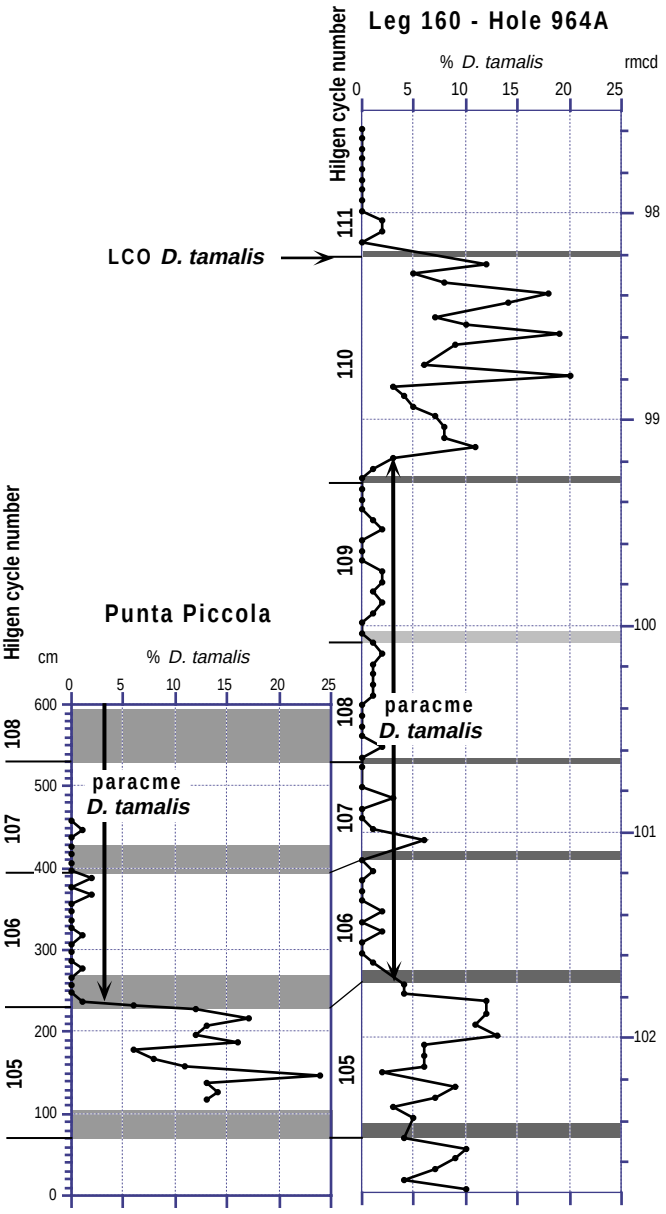

Figure 2. Abundance of *D. tamalis* in the Punta Piccola section and in Hole 964A.

In the Punta Piccola section, this biomarker corresponds (Di Stefano, pers. comm., 1996) to Driever's biohorizon d7, just below the sapropel base of cycle 11 (Driever, 1988), equivalent to Hilgen's cycle 106. Our observations confirm this stratigraphic position (Fig. 2). Therefore, sapropel 54 in Hole 964A appears to be equivalent to the base of cycle 106 at Punta Piccola.

These observations lead us to propose the equivalencies between Hole 964A and the Punta Piccola section that are shown in Table 1.

MINERALOGY

Hole 964A

Carbonate content (Fig. 3; Table 2) shows large cyclic variation (from 0% to 78.7%, mean = 62.0%) that is strongly correlated to the reflectance of the sediment: the lighter the sediment, the more carbonated. At 100.035 rmcd, there is a marked depletion in carbonate

percent (59.2%) that corresponds to a gray zone, but not to a sapropel. This depletion and the variation in the other mineral components led us to infer that this gray zone occurs in the place taken by sapropels in other cycles of the core.

Clay minerals can be classified into three groups, according to their abundance variations.

1. Palygorskite and kaolinite. The abundance of palygorskite ranges from 5.8% to 28.1% of the total of the clay minerals (mean = 20.5%). For kaolinite, these quantities are 8.7%, 20.6%, and 16.4%, respectively. The abundances are, on the whole, positively correlated to those of the carbonates.
2. Smectite and chlorite. The abundance of smectite ranges from 13.9% to 28.9% (mean = 19.3%). For chlorite, these quantities are 1.6%, 8.5%, and 4.1%, respectively. The two minerals show abundance variations opposite to that of palygorskite and kaolinite.
3. Illite and mixed-layer clay minerals. The abundance of illite ranges from 17.5% to 37.0% (mean = 24.9%). For mixed-layer clay minerals, these quantities are 11.1%, 17.8%, and 14.8%, respectively. Abundance variations of the two minerals do not show cyclicity, and illite abundance shows a weak upwards increase.

Table 1. Stratigraphical equivalences between Hole 964A and the Punta Piccola section.

Hole 964A sapropels	Punta Piccola cycles
50	111
51	110
Gray zone	109
52	108
53	107
54	106
55	105

Note: Punta Piccola cycles are from Hilgen (1991).

Quartz is not very abundant (6.6%–18.9% of the HCl insoluble fraction, mean = 13.0%). The abundance variation shows cycles correlated to those of palygorskite and kaolinite. Feldspars are present (1.1%–4.6% of the HCl insoluble fraction, mean = 2.9%, for the plagioclase; 1.0%–5.3%, mean = 2.9%, for the K-feldspar).Their abundance variations also show cycles that are positively correlated to those of palygorskite and kaolinite.

Punta Piccola Section

The sediments of the Punta Piccola section show variations in their mineralogical assemblage (De Visser et al., 1989; Foucault and Mélières, 1995) similar to those observed in Hole 964A (Fig. 4; Table 3). However, some differences can be seen.

The carbonate content shows cyclic variations; abundance minima occur in the gray beds. These variations (28.0%–62.0%, mean = 48.6%) are weaker than in Hole 964A. The abundance variations of palygorskite (1.2%–13.7%, mean = 7.0%) and kaolinite (8.3%–18.9%, mean = 13.6%) in this section are positively correlated to that of carbonate, as in Hole 964A. Smectite (14.9%–34.3%, mean = 25.0%) and chlorite (3.6%–11.8%, mean = 6.74%) abundance variations are negatively correlated to that of carbonate. Illite abundance variation, not cyclic in Hole 964A, shows a cyclic pattern similar to those of smectite and chlorite. K-feldspar, dolomite, and quartz abundances vary in the same way as kaolinite and palygorskite. Mixed-layer clay mineral abundances do not show cycles, but rather an increase towards the top of the section.

In conclusion, mineral abundance variations are very similar in Hole 964A and in the Punta Piccola section. In both sites, palygorskite and kaolinite abundance variations are positively correlated to carbonate content, whereas smectite and chlorite abundances vary in

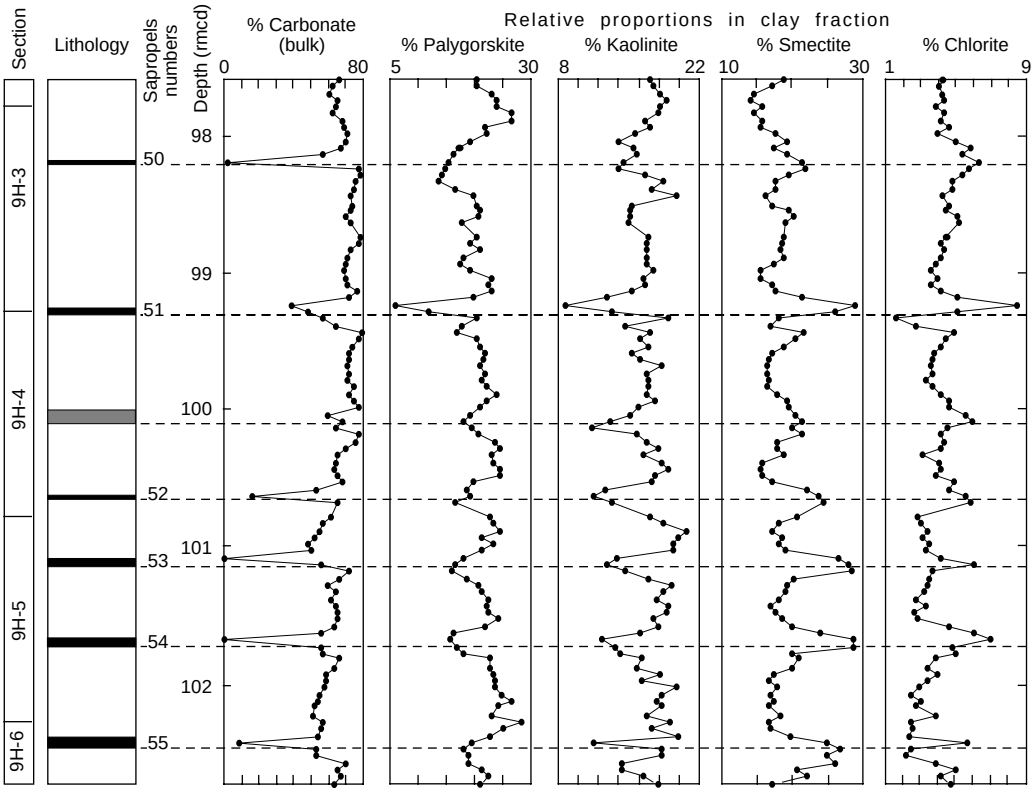

Figure 3. Lithology and mineral content of the sediment portion studied from Hole 964A. In lithology column, blank = nannofossil ooze; black = sapropels; gray = gray layer.

Table 2. X-ray mineralogy data, Hole 964A.

Core, section, interval (cm)	Depth (rmcd)	Carbonates (% in bulk)	Percentage in clay fraction						Percentage in carbonate-free fraction				
			Illite	Mixed-layer	Smectite	Chlorite	Kaolinite	Palygorskite	Quartz	Plagioclase	K- Feldspar	Pyrite	Goethite
160-964A-													
9H-2,130-131	97.585	65.7	27.8	11.8	18.7	4.3	17.1	20.4	12.5	3.2	4.7		
9H-2,135-136	97.635	62.6	25.6	15.6	17.2	4.0	17.4	20.3	15.0	3.6	4.2		
9H-2,140-141	97.685	60.7	25.7	14.4	14.6	4.2	18.1	23.0	14.3	3.5	3.8		
9H-2,145-146	97.735	64.7	25.6	13.6	14.0	4.3	18.8	23.8	13.9	3.8	3.6		
9H-3,0-1	97.785	64.5	26.6	11.9	15.7	3.8	18.0	23.9	13.9	3.3	3.6		
9H-3,5-6	97.835	62.1	25.2	11.8	14.5	4.3	17.8	26.4	14.0	3.8	3.9		
9H-3,10-11	97.885	67.8	25.6	11.7	15.6	4.1	16.6	26.5	13.0	2.7	2.7		
9H-3,15-16	97.935	68.8	27.3	13.9	15.5	4.6	17.0	21.8	12.0	2.4	3.0		
9H-3,20-21	97.985	70.9	27.7	13.2	17.6	4.0	15.6	22.0	11.0	3.3	2.4		
9H-3,25-26	98.035	69.5	27.1	15.6	19.1	5.0	13.9	19.2	10.8	2.3	1.9		
9H-3,30-31	98.085	67.0	29.7	14.6	17.3	5.8	15.4	17.1	10.1	2.4	2.2		
9H-3,35-36	98.135	57.0	30.7	13.0	19.1	5.3	15.8	16.2	6.6	1.2	1.4		13.5
9H-3,40-41	98.185	2.2	27.7	15.0	21.2	6.3	14.4	15.4	7.3	1.3	1.1		19.5
9H-3,46-47	98.245	77.4	26.2	17.5	21.7	5.8	14.0	14.9	11.8	2.7	2.2	2.0	
9H-3,50-51	98.285	78.3	29.6	15.0	19.4	5.3	16.5	14.3	12.2	3.0	1.9	1.7	
9H-3,55-56	98.335	75.6	32.8	12.8	17.6	4.8	18.4	13.6	12.1	3.1	3.0	2.6	
9H-3,60-61	98.385	74.8	30.0	13.9	17.5	4.8	17.3	16.5	13.8	3.2	3.1		
9H-3,65-66	98.435	72.6	25.0	15.0	16.2	4.2	19.7	19.8	13.0	3.0	2.6		
9H-3,72-73	98.505	73.7	25.7	17.1	17.1	4.6	15.3	20.2	13.9	2.9	2.7		
9H-3,75-76	98.535	72.7	25.8	14.3	19.5	4.4	15.1	20.9	14.0	3.5	2.9		
9H-3,80-81	98.585	70.1	24.2	15.0	20.1	5.1	15.1	20.6	13.3	3.2	2.9		
9H-3,85-86	98.635	72.9	29.3	13.8	19.0	5.2	15.0	17.8	10.8	2.6	2.1		
9H-3,95-96	98.735	77.8	25.8	14.0	18.7	4.4	16.9	20.3	11.6	2.4	2.3		
9H-3,100-101	98.785	77.4	27.6	14.0	18.4	4.1	16.8	19.1	11.8	2.6	2.7		
9H-3,105-106	98.835	73.0	26.0	14.0	18.2	4.3	16.8	20.9	14.2	2.9	2.0		
9H-3,110-111	98.885	70.9	27.5	14.9	18.8	4.1	16.8	17.9	15.4	3.6	3.4		
9H-3,114-115	98.935	69.8	29.8	15.0	17.3	3.8	16.8	17.3	13.5	3.2	3.9		
9H-3,120-121	98.985	68.8	31.1	13.4	15.5	3.5	17.4	19.1	11.4	3.0	3.2		
9H-3,125-126	99.035	69.6	26.7	14.8	15.3	3.9	16.4	22.9	13.4	3.2	2.8		
9H-3,130-131	99.085	71.1	25.0	15.3	17.1	3.5	16.6	22.5	12.1	3.0	2.6		
9H-3,135-136	99.135	75.9	24.0	16.0	17.6	4.1	15.3	23.0	13.2	2.4	2.0		
9H-3,140-141	99.185	71.6	25.9	15.3	21.4	5.0	12.7	19.6	12.1	2.5	1.7		
9H-3,145-146	99.235	38.4	37.0	11.1	28.9	8.5	8.7	5.8	13.5	3.9	1.7		
9H-4,0-1	99.285	48.3	27.5	16.4	26.0	5.1	13.4	11.7	8.9	1.7	1.0	3.3	
9H-4,5-6	99.335	56.1	25.6	15.8	18.0	1.6	18.8	20.2	9.2	1.7	2.2	0.8	
9H-4,10-11	99.385	64.4	32.9	15.4	16.8	2.7	14.5	17.6	16.0	4.9	5.3	1.5	
9H-4,15-16	99.435	78.7	25.2	14.5	21.5	4.8	17.1	16.8	13.1	3.2	2.1		
9H-4,20-21	99.485	76.9	24.0	15.0	20.4	4.4	16.1	20.2	14.3	3.2	3.6		
9H-4,25-26	99.535	73.3	23.9	15.4	18.7	4.1	16.9	21.0	13.5	3.3	3.3		
9H-4,30-31	99.585	71.8	25.4	16.7	17.2	3.7	15.3	21.7	14.2	3.8	3.4		
9H-4,35-36	99.635	71.2	27.2	15.0	16.6	3.7	16.1	21.4	14.5	3.9	4.0		
9H-4,40-41	99.685	70.2	28.4	12.8	16.3	3.6	18.2	20.8	14.0	3.4	4.6		
9H-4,45-46	99.735	71.6	26.7	14.8	16.4	3.6	16.7	21.8	15.5	3.7	3.7		
9H-4,50-51	99.785	70.9	27.8	14.1	16.7	3.3	16.9	21.2	14.1	3.5	3.4		
9H-4,55-56	99.835	74.3	27.8	13.1	16.4	3.6	17.0	22.1	13.5	3.3	3.2		
9H-4,60-61	99.885	71.9	22.6	15.0	17.7	4.1	16.8	23.8	12.7	3.1	3.0		
9H-4,65-66	99.935	74.8	22.4	14.1	19.2	4.6	17.6	22.1	12.5	3.2	2.6		
9H-4,70-71	99.985	77.1	24.2	14.8	19.5	4.6	16.0	20.9	13.1	3.1	2.7		
9H-4,75-76	100.035	59.2	23.8	16.0	20.5	5.5	15.0	19.2	10.8	2.4	2.2		
9H-4,80-81	100.085	67.7	26.4	15.4	21.3	5.9	13.2	17.9	11.2	2.2	1.9		
9H-4,85-86	100.135	64.2	30.6	14.4	20.0	4.5	11.3	19.3	17.1	4.6	5.3		
9H-4,90-91	100.185	77.3	23.4	15.0	21.3	4.1	15.7	20.5	12.2	2.5	2.4		
9H-4,95-96	100.235	75.1	22.8	15.0	17.9	4.3	16.7	23.4	12.7	2.8	2.6		
9H-4,100-101	100.285	69.3	22.6	13.2	17.9	4.1	17.9	24.4	11.9	2.9	2.8		
9H-4,105-106	100.335	64.9	22.6	16.4	18.6	3.1	16.4	22.8	11.9	2.5	2.2		
9H-4,110-111	100.385	63.8	24.3	14.6	15.7	4.0	18.2	23.2	13.1	3.1	3.6		
9H-4,115-116	100.435	63.5	23.7	13.3	15.5	4.1	18.9	24.5	13.8	3.6	4.0		
9H-4,120-121	100.485	64.7	25.3	13.3	15.6	3.8	17.5	24.6	13.3	3.3	3.4		
9H-4,125-126	100.535	67.9	27.2	14.1	17.0	4.8	17.3	19.7	12.1	2.8	2.5		
9H-4,130-131	100.585	53.2	24.6	17.6	22.0	4.6	12.7	18.5	10.9	2.6	1.8		
9H-4,135-136	100.635	16.4	27.5	12.7	23.6	5.5	11.5	19.2	10.5	2.6	1.8		
9H-4,140-141	100.685	65.0	23.4	16.5	24.4	5.8	13.3	16.6	12.4	2.8	1.7	2.4	
9H-5,0-1	100.785	60.8	21.4	15.4	20.7	2.8	17.1	22.6	14.3	3.0	3.3		
9H-5,5-6	100.835	56.9	21.4	15.9	18.0	3.0	18.4	23.4	13.3	2.7	2.9		
9H-5,10-11	100.885	54.9	21.5	13.0	17.1	3.3	20.6	24.5	15.4	3.2	3.3		
9H-5,15-16	100.935	52.2	21.4	15.8	18.5	3.1	19.9	21.3	16.4	3.6	4.2		
9H-5,20-21	100.985	47.7	21.7	14.2	18.1	3.4	19.4	23.1	14.8	3.1	3.6		
9H-5,25-26	101.035	49.6	23.4	14.0	19.0	3.2	19.3	21.1	14.1	3.1	3.1		
9H-5,30-31	101.085	0.2	19.9	17.8	26.5	4.1	13.8	17.9	10.3	1.8	1.4		
9H-5,35-36	101.135	55.8	21.0	15.9	28.0	6.0	12.7	16.4	13.8	3.3	1.9	2.9	
9H-5,40-41	101.185	71.2	22.0	15.5	28.3	3.7	14.5	16.1	13.1	2.4	2.4	1.8	
9H-5,45-46	101.235	65.5	24.7	16.2	20.0	3.5	16.9	18.6	15.5	3.9	4.3	2.7	
9H-5,50-51	101.285	59.8	22.6	14.9	19.2	3.3	19.3	20.7	13.4	3.2	3.1	3.7	
9H-5,55-56	101.335	64.0	22.7	15.5	19.1	3.1	18.5	21.1	16.6	3.6	4.5	3.1	
9H-5,60-61	101.385	60.9	21.2	18.1	18.1	2.7	17.7	22.2	15.2	3.0	3.3	1.3	
9H-5,65-66	101.435	64.0	23.9	15.1	16.9	3.2	18.9	22.0	14.8	3.3	3.7	1.3	
9H-5,70-71	101.485	64.9	25.6	13.3	17.5	2.6	18.8	22.3	14.2	2.9	3.2	3.1	
9H-5,75-76	101.535	65.0	21.4	15.8	18.4	2.8	17.4	24.2	12.7	2.9	3.3	5.0	
9H-5,80-81	101.585	63.5	22.3	13.6	19.9	4.5	17.9	21.9	13.0	3.2	1.7	2.0	
9H-5,85-86	101.635	55.4	22.8	15.2	23.8	6.0	16.1	16.2	11.7	2.3	1.1		
9H-5,90-91	101.685	0.0	23.4	13.2	28.7	6.9	12.3	15.5	9.7	1.1	0.7	5.0	
9H-5,95-96	101.735	55.7	21.9	14.5	28.5	4.8	13.6	16.8	10.8	1.7	1.0	3.7	
9H-5,100-101	101.785	56.8	27.9	15.3	19.9	4.9	14.0	18.0	16.4	3.8	3.4	8.6	
9H-5,103-104	101.815	66.1	21.6	14.8	20.9	3.8	16.2	22.7	13.5	2.4	2.5	3.2	
9H-5,110-111	101.885	63.3	22.6	15.8	19.9	3.3	15.8	22.6	15.4	2.8	3.6	1.8	
9H-5,115-116	101.935	58.5	21.1	16.4	17.4	4.0	18.0	23.1	15.8	3.0	3.6	0.6	
9H-5,120-121	101.985	58.6	23.0	17.2	16.7	3.3	16.2	23.6	13.4	2.6	2.9		

Table 2 (continued).

Core, section, interval (cm)	Depth (rmcd)	Carbonates (% in bulk)	Percentage in clay fraction						Percentage in carbonate-free fraction				
			Illite	Mixed-layer	Smectite	Chlorite	Kaolinite	Palygorskite	Quartz	Plagioclase	K- Feldspar	Pyrite	Goethite
9H-5,125-126	102.035	57.8	21.2	14.6	17.9	2.9	19.7	23.7	16.7	3.8	4.0		
9H-5,130-131	102.085	54.9	22.4	15.3	16.7	2.4	18.3	24.9	16.3	3.1	4.3		
9H-5,135-136	102.135	53.7	21.6	14.0	17.3	3.0	17.7	26.5	14.0	3.2	3.6		
9H-5,138-139	102.165	52.3	21.6	16.5	16.7	2.7	18.2	24.3	15.3	3.7	4.0		
9H-5,145-146	102.235	50.5	21.1	17.2	18.2	3.8	16.7	22.9	11.6	2.6	2.4		
9H-6,0-1	102.285	56.6	17.5	16.4	16.6	2.4	19.1	28.1	9.0	1.8	2.3		
9H-6,5-6	102.335	55.5	22.8	15.8	16.7	2.5	17.2	25.0	12.2	2.9	3.6		
9H-6,10-11	102.385	53.7	21.7	13.8	19.7	2.3	19.9	22.6	10.6	2.4	3.1	2.8	
9H-6,15-16	102.435	8.1	21.0	17.6	24.7	5.6	11.5	19.6	12.5	2.3	1.7	3.4	
9H-6,20-21	102.485	52.7	20.5	14.1	26.7	2.5	18.3	18.0	7.5	1.5	1.6	2.7	
9H-6,25-26	102.535	52.6	19.0	17.0	24.9	2.2	18.2	18.8	7.6	1.5	2.0	1.0	
9H-6,30-31	102.585	70.1	22.0	14.9	26.0	3.8	14.3	18.9	10.9	2.7	2.6	4.3	
9H-6,35-36	102.635	65.1	24.0	15.2	20.6	4.9	14.3	21.1	18.9	4.5	4.5	0.5	
9H-6,40-41	102.685	67.1	20.4	14.6	22.1	4.1	16.5	22.3	14.6	3.3	3.2		
9H-6,45-46	102.735	63.1	22.3	17.2	17.0	4.6	17.9	21.0	14.7	3.5	3.3		

Notes: rmcd = revised meter composite depth. Carbonates (percentage in bulk) from manocalcimetry.

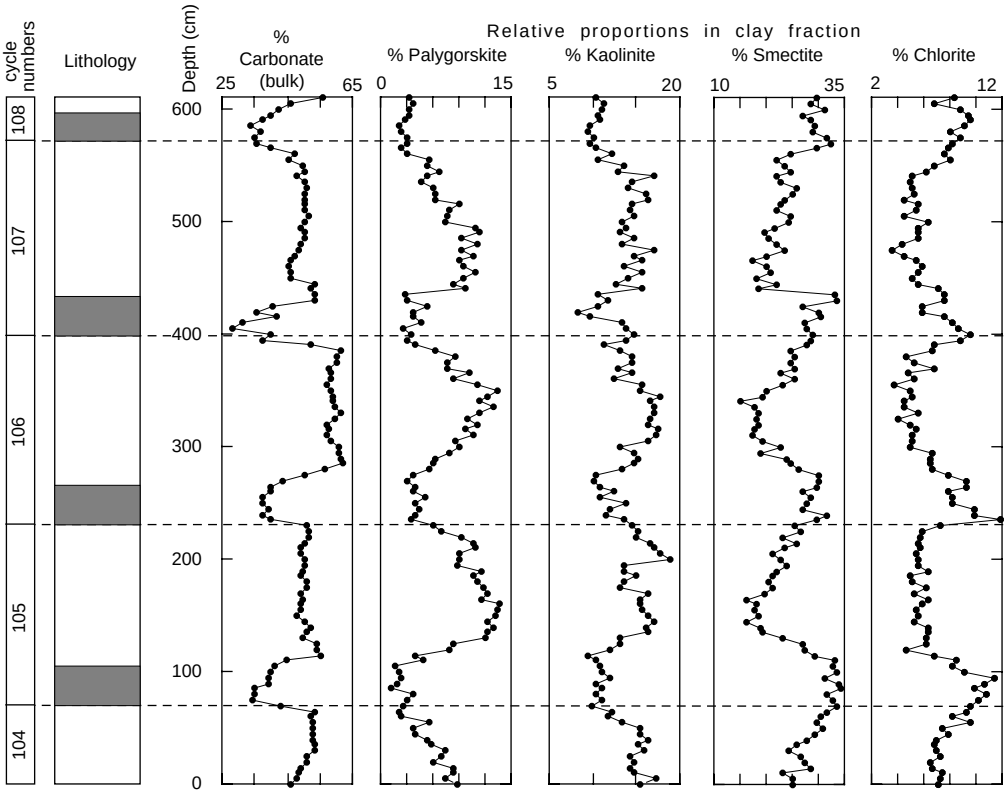

Figure 4. Lithology and mineralogical content of cycles 104 to 108 (Hilgen, 1991) at Punta Piccola. In lithology column, blank = carbonate-rich marls; gray = gray layers.

opposite ways. These similarities suggest that the same sedimentation processes acted at the two sites. However, palygorskite and kaolinite are much more abundant at Hole 964A than in Sicily, which may correspond to different contributions from sources areas

INTERPRETATION

One of the more characteristic minerals, among the ones analyzed, is palygorskite, because the only significant source area for this mineral, in this part of the central Mediterranean, is Africa. On this continent, Paleogene sediments are known to be palygorskite rich. This mineral is commonly found in Senegal, Ivory Coast, Dahomey, Sudan, Morocco (Millot, 1963), Algeria, and Tunisia, as well as in the southern Saharan Atlas (Chamley, 1971; Sassi, 1974; Coudé-Gaussen, 1991). Actually, along the Algerian-Tunisian coast, North Africa yields palygorskite to marine sediments that show a decreasing abundance gradient of this mineral seaward (Blanc-Vernet et al., 1975; Burollet et al., 1979). However, sea transportation of palygorskite from Africa to Site 964 or to the Sicilian coast does not seem possible because of the strong surface current flowing through the Siculo-Tunisian strait from north–west to south–east, acting as a hydrodynamic barrier. A wind transportation process, attested to by many direct observations (Coudé-Gaussen, 1991; Bergametti et al., 1989), seems to be the only explanation available. In the Western Mediterranean area, some Quaternary continental formations con-

Table 3. X-ray mineralogy data, Punta Piccola section.

Depth (cm)	Percentage in bulk			Percentage in clay fraction						Percentage in carbonate-free fraction		
	Carbonates	Calcite	Dolomite	Illite	Mixed-layer	Smectite	Chlorite	Kaolinite	Palygorskite	Quartz	K-Feldspar	Plagioclase
2.5	46.0	43.5	2.27	29.1	14.8	24.9	7.1	15.4	8.7	13.6	2.2	2.8
7.5	47.5	44.8	2.57	29.7	13.4	24.9	7.3	17.3	7.4	12.0	2.1	2.8
12.5	48.5	46.4	2.02	30.0	16.5	23.1	7.4	14.8	8.2	13.7	2.2	3.0
17.5	49.0	47.1	1.92	26.7	16.0	28.3	6.6	14.2	8.2	12.0	1.9	2.6
22.5	51.0	48.7	2.23	28.6	16.9	27.2	6.5	14.7	6.1	14.0	2.3	3.2
27.5	51.0	48.6	2.31	30.1	14.8	26.6	7.2	14.3	7.0	14.3	2.5	3.0
32.5	53.5	51.7	1.23	29.4	16.0	24.4	6.9	15.9	7.4	12.7	2.0	2.6
37.5	53.0	51.3	1.88	30.3	16.3	25.7	6.7	15.2	5.8	13.6	1.7	3.0
42.5	52.5	50.8	1.75	29.3	14.6	27.6	6.9	16.4	5.2	13.9	1.7	2.7
47.5	52.5	50.9	1.60	28.9	14.6	29.2	7.9	15.4	4.0	13.3	1.9	3.0
52.5	52.5	50.3	2.16	27.0	15.8	30.8	7.4	15.4	3.6	13.6	1.5	2.6
57.5	52.5	51.2	1.32	25.0	16.9	29.7	9.6	13.2	5.6	14.4	1.5	2.8
62.5	52.0	51.1	1.13	27.9	19.3	30.5	8.1	11.8	2.4	13.7	1.4	2.7
67.5	53.0	51.7	1.28	26.5	18.4	31.6	9.3	12.1	2.1	12.6	1.1	2.8
72.5	43.0	41.0	2.02	28.0	16.8	33.3	9.5	9.8	2.6	12.5	1.2	2.7
77.5	34.0	32.2	1.85	27.7	15.5	32.8	10.1	11.0	3.0	12.9	1.2	2.3
82.5	35.0	33.2	1.74	28.3	15.3	31.5	10.8	10.3	3.8	14.4	1.6	2.6
87.5	35.0	33.1	2.02	27.6	16.1	34.3	9.8	11.0	1.2	12.9	1.5	2.7
92.5	39.0	37.2	1.83	26.7	16.8	33.8	10.6	10.3	1.8	13.6	1.3	2.7
97.5	39.0	37.3	1.83	25.4	17.9	31.1	11.4	11.9	2.2	14.3	1.4	3.2
102.5	40.0	38.3	1.66	25.5	19.2	33.3	9.1	10.9	2.0	11.8	1.4	2.4
107.5	41.0	39.5	1.50	26.1	20.9	32.6	8.1	10.7	1.6	12.5	0.9	2.3
112.5	44.5	42.9	1.77	26.7	16.7	33.0	8.5	10.3	4.8	12.9	1.1	2.3
117.5	55.0	54.0	1.08	28.6	22.2	29.1	6.7	9.4	4.0	12.4	1.4	2.5
122.5	54.0	53.1	1.08	27.6	20.7	27.4	4.6	11.9	7.8	12.4	1.4	2.7
127.5	54.0	52.9	1.18	28.5	17.7	26.9	6.1	13.1	8.2	13.1	1.6	2.8
132.5	49.5	47.8	1.93	27.1	18.3	23.2	6.2	13.1	12.1	13.8	2.2	2.7
137.5	51.0	49.4	1.96	28.1	18.0	19.1	6.3	16.3	12.2	13.2	2.1	2.6
142.5	52.0	50.1	1.89	28.8	17.2	18.7	6.3	16.1	12.9	12.8	2.4	2.4
147.5	50.5	48.6	2.10	30.2	19.2	16.3	5.2	16.9	12.2	13.5	2.4	2.9
152.5	48.0	45.8	2.34	28.4	18.2	18.4	5.5	16.3	13.2	15.0	3.3	2.8
157.5	49.0	47.5	2.12	30.8	17.2	17.7	5.4	15.6	13.3	14.8	3.2	3.1
162.5	49.0	46.8	2.46	28.9	18.2	18.0	5.8	15.3	13.7	13.9	2.8	3.3
167.5	49.5	47.9	2.05	30.8	19.9	16.1	6.3	15.3	11.6	14.0	2.0	2.4
172.5	49.0	47.2	2.44	27.3	19.1	19.6	5.3	16.4	12.3	14.8	2.4	3.0
177.5	51.0	48.7	2.40	29.4	18.6	21.0	6.1	13.1	11.8	14.2	2.7	2.0
182.5	51.0	48.2	2.65	31.0	19.2	20.2	5.0	13.6	11.0	12.6	2.1	2.2
187.5	49.0	46.6	2.59	29.2	19.2	21.3	4.9	14.9	10.5	13.0	2.6	2.7
192.5	49.5	46.6	2.91	27.1	19.6	21.8	6.3	13.6	11.6	12.4	2.3	2.2
197.5	50.0	47.3	2.60	27.4	20.7	24.0	5.6	13.5	8.8	11.9	2.2	2.1
202.5	50.0	48.5	2.29	27.5	16.2	22.8	5.5	18.9	9.1	14.9	1.9	2.2
207.5	49.0	47.7	2.07	28.9	17.6	21.3	5.4	17.8	9.0	15.6	2.3	2.8
212.5	49.0	47.5	2.43	27.7	15.3	23.3	5.7	17.1	10.9	15.6	2.2	2.9
217.5	50.5	48.7	1.84	23.9	17.8	25.6	5.6	16.6	10.5	16.1	2.0	2.8
222.5	51.5	49.9	1.65	25.8	21.4	22.9	5.7	14.9	9.3	14.9	1.8	2.3
227.5	51.5	50.7	1.65	23.0	22.3	26.7	5.9	15.2	6.9	13.2	1.5	2.3
232.5	51.0	49.5	1.54	25.6	21.4	25.4	7.2	14.4	6.0	14.0	1.3	2.9
237.5	39.5	38.7	1.92	24.9	16.7	29.6	11.8	13.6	3.4	14.2	1.5	2.6
242.5	37.0	35.2	1.96	22.8	20.4	31.6	9.9	11.4	3.9	12.7	0.7	2.4
247.5	39.0	37.2	1.92	26.1	20.8	27.1	9.8	11.9	4.3	11.1	0.8	2.2
252.5	37.0	35.7	1.99	26.2	20.3	27.6	8.2	13.8	3.9	12.4	1.6	2.9
257.5	37.0	35.8	1.73	26.2	21.3	28.6	8.1	10.7	5.1	11.4	1.2	2.8
262.5	40.0	39.7	1.96	25.0	24.2	26.8	7.8	12.4	3.8	13.9	1.7	3.0
267.5	39.5	38.2	1.54	25.6	20.5	29.8	9.3	10.8	4.0	14.1	1.2	2.5
272.5	43.5	42.0	1.67	24.8	22.9	30.1	9.3	10.0	2.9	14.4	1.4	2.8
277.5	50.0	48.7	1.45	26.1	22.1	30.0	7.9	10.3	3.6	15.5	1.7	3.2
282.5	56.5	55.4	1.46	25.9	22.3	26.3	6.6	13.3	5.6	12.4	1.4	2.1
287.5	62.0	61.2	1.03	24.3	24.0	24.7	6.4	14.7	5.9	13.0	1.3	2.3
292.5	61.0	59.9	1.32	26.0	22.4	23.7	6.5	15.1	6.3	12.4	1.2	2.1
297.5	60.5	58.9	1.70	29.8	22.2	19.0	6.6	14.6	7.8	14.1	1.8	3.0
302.5	60.5	59.5	1.61	27.4	23.1	22.5	4.9	13.1	9.0	14.3	1.4	2.6
307.5	58.5	56.7	1.90	31.8	19.2	19.1	5.0	16.3	8.6	16.0	2.9	3.7
312.5	57.0	56.9	1.15	28.3	21.7	17.2	5.0	17.2	10.6	15.2	2.2	3.1
317.5	57.5	56.3	1.25	31.3	18.4	17.8	5.4	17.4	9.7	13.0	1.6	2.7
322.5	57.0	56.0	1.05	27.4	21.9	18.4	4.9	16.3	11.1	14.8	1.9	3.2
327.5	59.5	58.5	1.62	28.3	23.0	18.1	4.0	16.6	10.0	15.3	2.5	2.9
332.5	61.0	59.4	1.57	29.0	18.6	18.6	5.6	16.9	11.3	14.0	2.3	2.7
337.5	59.5	57.7	1.78	30.7	17.3	17.7	4.4	16.9	13.0	14.6	2.8	2.9
342.5	59.0	56.9	2.05	30.3	22.5	14.9	4.4	16.6	11.3	13.0	2.0	2.2
347.5	59.0	57.1	1.88	25.5	20.1	19.3	5.1	17.8	12.2	13.3	1.8	2.9
352.5	58.0	56.0	2.02	23.8	22.7	19.9	4.9	15.3	13.4	15.0	2.1	2.8
357.5	57.0	54.7	2.34	23.8	22.6	23.1	3.7	15.7	11.1	12.8	2.7	2.4
362.5	58.5	57.6	1.46	25.7	23.3	25.2	5.3	12.3	8.2	13.3	1.6	2.0
367.5	58.0	55.8	2.18	26.2	21.8	22.7	4.8	14.4	10.1	14.4	1.5	2.8
372.5	57.5	55.9	1.70	24.8	22.8	25.2	6.8	12.8	7.6	13.4	1.5	2.5
377.5	60.0	58.3	1.88	26.4	21.8	24.5	5.2	14.5	7.6	15.5	1.8	2.9
382.5	60.0	58.5	1.49	24.1	23.0	25.3	4.6	14.5	8.5	13.0	1.4	2.0
387.5	61.0	59.8	1.14	24.4	25.2	24.6	6.6	13.0	6.2	12.8	1.5	2.2
392.5	52.0	51.6	1.33	22.3	28.0	27.8	6.7	11.2	4.0	13.2	1.3	2.9
397.5	37.0	35.5	1.55	22.8	23.3	28.4	8.7	13.8	3.0	12.9	1.0	2.3
402.5	39.5	24.2	1.50	24.1	19.3	29.0	9.6	14.6	3.4	11.4	0.9	2.4
407.5	28.0	26.3	1.79	24.3	23.2	27.5	8.6	13.8	2.6	12.6	1.0	2.3
412.5	31.0	29.3	1.82	23.8	22.9	27.4	8.2	13.2	4.5	11.4	0.9	2.2
417.5	41.5	35.3	1.93	24.7	23.7	30.5	7.6	9.7	3.8	12.4	1.0	2.6
422.5	35.5	34.3	1.29	25.0	27.1	30.0	5.9	8.3	3.7	11.2	1.1	2.1
427.5	40.5	39.0	1.60	22.9	28.2	27.1	5.9	10.5	5.4	11.6	1.1	2.3
432.5	53.0	51.9	1.41	24.8	19.3	33.6	7.6	11.8	2.9	11.6	1.7	2.3
437.5	53.5	52.5	1.31	24.5	21.8	32.9	7.5	10.6	2.7	11.3	1.2	2.2

Table 3 (continued).

Depth (cm)	Percentage in bulk			Percentage in clay fraction						Percentage in carbonate-free fraction		
	Carbonates	Calcite	Dolomite	Illite	Mixed-layer	Smectite	Chlorite	Kaolinite	Palygorskite	Quartz	K-Feldspar	Plagioclase
442.5	52.0	49.7	2.22	26.8	22.5	18.3	7.0	15.6	9.8	12.6	2.1	2.6
447.5	53.0	51.6	1.43	27.6	23.8	22.1	5.5	12.6	8.4	11.3	1.9	2.4
452.5	46.0	43.6	2.49	29.4	24.2	17.9	5.0	14.0	9.5	13.6	2.3	2.6
457.5	46.0	44.1	2.01	28.0	19.0	20.9	5.5	15.7	10.9	12.5	2.0	2.7
462.5	45.5	43.4	2.32	27.3	23.8	20.0	5.9	13.6	9.4	14.7	2.2	2.7
467.5	46.0	43.1	3.03	30.6	22.1	17.3	5.4	15.5	9.1	12.8	2.6	3.0
472.5	47.0	44.9	2.20	24.8	25.6	20.0	4.4	14.6	10.6	14.4	2.1	2.6
477.5	48.5	46.4	2.11	27.2	19.7	23.3	3.6	17.0	9.2	13.9	2.6	2.8
482.5	49.0	46.7	2.46	23.4	26.0	22.0	4.3	13.3	11.0	12.3	2.0	2.2
487.5	50.0	47.4	2.48	25.6	24.6	20.4	5.5	14.7	9.2	14.2	2.1	2.3
492.5	50.5	48.5	2.16	25.2	25.4	19.6	5.6	13.0	11.2	13.3	1.9	2.0
497.5	49.0	47.5	1.83	24.2	23.9	21.6	5.6	13.8	10.9	14.3	2.2	2.6
502.5	50.0	47.8	2.26	24.6	24.1	24.4	6.3	13.2	7.4	13.2	2.0	2.3
507.5	51.5	50.1	1.52	24.7	24.1	24.6	4.5	14.6	7.5	14.6	1.7	2.9
512.5	50.5	48.2	2.34	23.5	27.1	21.8	5.4	14.3	7.9	14.3	2.0	2.2
517.5	50.0	47.5	2.52	25.2	23.1	22.6	5.6	14.4	9.1	14.0	1.9	2.5
522.5	50.5	48.7	1.98	24.6	24.9	23.5	4.4	16.3	6.3	13.5	1.3	2.0
527.5	50.0	48.7	1.58	22.2	25.2	24.9	5.3	16.1	6.3	13.8	1.5	2.6
532.5	51.0	49.1	1.77	25.6	24.0	25.6	5.0	13.9	5.9	13.6	1.7	2.0
537.5	50.0	48.1	2.02	23.4	29.9	22.8	4.9	14.4	4.6	14.9	1.2	2.1
542.5	48.0	45.6	2.38	24.7	26.0	21.9	5.1	17.0	5.3	13.0	1.2	1.8
547.5	50.0	48.1	2.06	22.9	26.6	24.8	6.2	12.8	6.7	14.8	1.4	2.1
552.5	49.5	48.1	1.61	23.1	27.8	23.5	6.7	13.7	5.2	13.8	1.4	2.0
557.5	45.0	43.5	1.53	27.8	25.9	22.1	8.0	10.6	5.6	12.4	1.3	2.2
562.5	47.0	45.4	1.62	24.5	28.1	24.7	7.6	12.1	3.0	14.1	1.2	2.0
567.5	40.0	38.0	1.96	26.0	24.0	29.6	7.8	10.2	2.4	14.3	1.4	2.5
572.5	35.5	33.5	1.99	25.0	22.0	32.3	8.1	9.7	2.9	14.2	0.9	2.6
577.5	35.0	33.1	1.87	24.3	22.2	31.6	8.8	10.1	3.0	13.4	0.9	2.3
582.5	36.5	35.1	1.59	25.3	26.0	29.0	8.0	9.3	2.4	13.6	1.2	2.3
587.5	33.5	31.1	2.38	25.7	24.3	29.1	9.1	9.7	2.1	11.8	0.8	2.4
592.5	37.5	35.6	1.92	26.9	21.5	28.5	9.6	10.8	2.7	12.3	0.8	2.1
597.5	39.5	38.0	1.57	25.7	24.0	27.1	9.4	10.5	3.3	11.9	0.8	2.1
602.5	42.0	40.6	1.59	24.5	21.5	31.0	8.8	10.9	3.3	13.2	0.7	2.3
607.5	46.0	44.8	1.30	25.4	24.5	28.4	6.7	11.3	3.7	13.6	0.8	2.5
612.5	55.5	54.1	1.39	25.1	23.5	29.5	8.3	10.3	3.3	13.8	0.9	2.3

Note: Carbonates (percentage in bulk) from manocalcimetry.

firm this mechanism. In South Tunisia, thick peridesertic loess-like palygorskite-rich formations resting on the Matmata plateau have an eolian origin from the Sahara (Coudé-Gaussen, 1990), and the occurrence of palygorskite in Corsican Holocene lake deposits cannot be explained except by a wind contribution from the African continent (Robert et al., 1984).

We then hypothesize that the wind transported palygorskite from Africa to the locations of Site 964 and Punta Piccola. If this hypothesis is correct, kaolinite, quartz, and feldspar, whose variations are positively correlated to these of palygorskite, must have the same origin. This is confirmed by the observation that these minerals are associated today with wind-blown dust from Africa (Bergametti et al., 1989).

Smectite and chlorite show variations opposite to those of palygorskite and kaolinite and therefore must be different in origin. Areas located at the north of Mediterranean basin may act as sources for these minerals through fluvial erosion. Several formations outcropping in Sicily contain large amounts of smectite (Chamley, 1976). Chlorite is abundant in the metamorphic terranes of alpine framework bordering the Mediterranean at the north.

Because of the wind transportation of palygorskite, its cyclic abundance variation may be explained by an identical cyclic variation of wind strength. But another phenomenon may have a more important influence upon eolian erosion. We know that during recent periods, within ~6 ka, an increase in precipitation on the Sahara and peri-Saharan areas resulted in a spreading of vegetation (Street-Perrott and Perrott, 1993). This vegetation may completely stop the eolian erosion processes and the exportation of eolian palygorskite, kaolinite, and related minerals out of Africa.

So we suggest that the cyclic variation of the mineral composition at Hole 964A and at Punta Piccola results from the alternation of weak and strong rainfall periods on both south and north Mediterranean sides as follows.

1. **Periods of minimum rainfall.** On the south side of the Mediterranean, a weakening of rainfall increased the aridity of the Sahara, resulting in a reduced and scattered vegetation in peri-Saharan areas. Consequently, soils were far more vulnerable to wind erosion, which led to an increased wind transportation of minerals (palygorskite, kaolinite, dolomite, quartz, potassium feldspar, and dolomite) from these areas to the Mediterranean. On the northern side of the Mediterranean, a decrease of rainfall resulted not only in a decrease in the river discharge, but also in the sediment load, because fluvial erosion lost its efficiency. Consequently, the detrital material supply of rivers to the sea decreased, increasing the concentration of wind-transported material in the sediment. During these periods, sediments show the highest content in palygorskite and related minerals (kaolinite, dolomite, quartz, and feldspar) and the lowest in smectite and chlorite.
2. **Periods of maximum rainfall.** On the south side of the Mediterranean, an increase in rainfall on the Sahara, as well as on peri-Saharan areas, allowed the vegetation to spread over, protecting soils and significantly reducing, or even stopping, the eolian erosion. On the north side of the Mediterranean, an increase in rainfall did not notably modify the density of pre-existent vegetation, but resulted in an increase in river erosion. Consequently, the sediment yield increased with river discharge and provided more terrigenous supply to marine sedimentation. During these periods, sediments show the highest content in smectite and chlorite. Sapropel or gray bed deposition occurs during these periods.

CONCLUSION

The Pliocene sedimentation in the Ionian Basin (Hole 964A) and at Punta Piccola shows outstanding similarities. At both places, cyclic sedimentation is mostly characterized by abundance variations of most of the mineral constituents. These variations are interpreted as the result of cyclic climatic changes that controlled eolian and river sedimentation processes.

During dry periods, the Saharan and peri-Saharan soils are unprotected because of the scarcity of the vegetation. Therefore, eolian erosion pulls away palygorskite, kaolinite, and associated minerals, which are carried over the central Mediterranean to the Ionian Basin and Sicily.

During humid periods, the presence of a vegetative cover on the Sahara and peri-Saharan areas prevents the eolian erosion. Consequently, palygorskite, kaolinite, and associated minerals are no longer carried over the Mediterranean, whereas the Alpine terrigenous contribution marked by chlorite and smectite is enhanced because of strong fluvial erosion.The sapropels of the Ionian Basin and gray beds of Punta Piccola occur during these humid periods.

ACKNOWLEDGMENTS

We thank Fabio Trincardi and Belén Alonso for their critical and useful reviews.

REFERENCES

Bergametti, G., Gomes, L., Remoudaki, E., Desbois, M., Martin, D., and Buat-Ménard, P., 1989. Present transport and deposition patterns of African dust to the North-Western Mediterranean. *In* Leinen, M., and Sarthein, M. (Eds.), *Paleoclimatology and Paleometeorology: Modern and Past Patterns of Global Atmospheric Transport:* Dordrecht (Kluwer Academic), 227–252.

Blanc-Vernet, L., Chamley, H., Froget, C., Le Boulicault, D., Monaco, A., and Robert, C., 1975. Observations sur la sédimentation marine récente dans la région siculo-tunisienne. *Geol. Mediterr.,* 2:31–48.

Brolsma, M.J., 1978. Quantitative foraminiferal analysis and environmental interpretation of the Pliocene and topmost Miocene on the South coast of Sicily. *Utrecht Micropaleontol. Bull.,* 18:1–159.

Burollet, P.F., Clairefond, P., and Winnock, E. (Eds.), 1979. La mer Pélagienne. *Geol. Mediterr.,* 6:1–345.

Chamley, H., 1971. Recherches sur la sedimentation argileuse en Méditerranée. *Sci. Geol. Mem.,* 35.

Channell, J.E.T., Di Stefano, E., and Sprovieri, R., 1976. Minéralogie des argiles, lithologie et tectonique dans le Pliocène du Capo Rossello (Sicile). *C.R. Somm. Soc. Geol. Fr.,* 39–41.

————, 1992. Calcareous plankton biostratigraphy, magnetostratigraphy and paleoclimatic history of the Plio-Pleistocene Monte S. Nicola section (Southern Sicily). *Boll. Soc. Paleontol. Ital.,* 31:351–382.

Coudé-Gaussen, G., 1990. The loess and loess-like deposits along the sides of the Western Mediterranean Sea: genetic and paleoclimatic significance. *Quat. Int.,* 5:1–8.

————, 1991. Les poussières sahariennes: France (John Libbey Eurotext).

De Visser, J.P., Ebbing, J.H.J., Gudjonsson, L., Hilgen, F.J., Jorissen, F.J., Verhallen, P.J.J.M., and Zevenboom, D., 1989. The origin of rhythmic bedding in the Pliocene Trubi formation of Sicily, southern Italy. *Palaeogeogr., Palaeoclimatol., Palaeoecol.,* 69:45–66.

Driever, B.W.M., 1988. Calcareous nannofossil biostratigraphy and paleoenvironmental interpretation of the Mediterranean Pliocene. *Utrecht Micropalaeontol. Bull.,* 36:1–245.

Foucault, A., and Mélières, F., 1995. Nature et origine des cycles sédimentaires métriques du Pliocène de l´Ouest méditerranéen d´après l´étude du contenu terrigène de la Formation Narbone (Punta Piccola, Sicile, Italie). *C. R. Acad. Sci. Paris,* 321:869–876.

Hilgen, F.J., 1987. Sedimentary rhythms and high-resolution chronostratigraphic correlations in the Mediterranean Pliocene. *Newsl. Stratigr.,* 17:109–127.

————, 1991. Extension of the astronomically calibrated (polarity) time scale to the Miocene/Pliocene boundary. *Earth Planet. Sci. Lett.,* 107:349–368.

Lourens, L.J., Antonarakou, A., Hilgen, F.J., Van Hoof, A.A.M., Vergnaud-Grazzini, C., and Zachariasse, W.J., 1996. Evaluation of the Plio-Pleistocene astronomical timescale. *Paleoceanography,* 11:391–413.

Mélières, F., 1973. Porte-échantillon tournant pour analyse par diffractométrie X. *Bull. Soc. Fr. Mineral. Cristallogr.,* 96:75–79.

Millot, G., 1963. *Géologie des Argiles:* Paris (Masson).

Rio, D., Raffi, I., and Villa, G., 1990. Pliocene-Pleistocene calcareous nannofossil distribution patterns in the Western Mediterranean. *In* Kastens, K.A., Mascle, J., et al., *Proc. ODP, Sci. Results,* 107: College Station, TX (Ocean Drilling Program), 513–533.

Robert, C., Gauthier, A., and Chamley, H., 1984. Origine autochtone et allochtone des argiles récentes de haute altitude en Corse. *Geol. Mediterr.,* 11:243–253.

Sassi, S., 1974. La sédimentation phosphatée au Paléocène dans le Sud et le Centre-Ouest de la Tunisie [Thèse Sci.]. Nat. Univ. Paris-Sud.

Shipboard Scientific Party, 1996. Site 964. *In* Emeis, K.-C., Robertson, A.H.F., Richter, C., et al., *Proc. ODP, Init. Repts.,* 160: College Station, TX (Ocean Drilling Program), 85–123.

Sprovieri, R., Di Stefano, E., Riggi, A., and Busalacchi, P., 1994. La sezione intra-pliocenica di Gibil-Gabel (Caltanissetta, Sicilia centrale): un esercizio di biostratigrafia ad alta risoluzione. *Boll. Soc. Paleont. It.,* 33:289–298.

Street-Perrott, F.A., and Perrott, R.A., 1993. Holocene vegetation, lake levels, and climate of Africa. *In* Wright, H.E., Jr., Kutzbach, J.E., Webb, III, T., Ruddiman, W.F., Street-Perrott, F.A., and Bartlein, P.J. (Eds.), *Global Climate Since the Last Glacial Maximum:* Minneapolis (Univ. Minnesota Press), 318–356.

Van Os, B.J.H., Lourens, L.J., Hilgen, F.J., de Lange, G.J., and Beaufort, L., 1994. The formation of Pliocene sapropels and carbonate cycles in the Mediterranean: diagenesis, dilution, and productivity. *Paleoceanography,* 9:601–617.

Date of initial receipt: 22 January 1997
Date of acceptance: 24 June 1997
Ms 160SR-012

Prior Chapter Contents Next Chapter